J Biol Phys (2016) 42:477–502
DOI 10.1007/s10867-016-9418-3

ORIGINAL PAPER

Spatio-temporal morphology changes in and quenching effects on the 2D spreading dynamics of cell colonies in both plain and methylcellulose-containing culture media

N. E. Muzzio[1] · M. A. Pasquale[1] · M. A. C. Huergo[1] · A. E. Bolzán[1] · P. H. González[2] · A. J. Arvia[1]

Received: 21 September 2015 / Accepted: 4 April 2016 / Published online: 7 June 2016

Abstract To deal with complex systems, microscopic and global approaches become of particular interest. Our previous results from the dynamics of large cell colonies indicated that their 2D front roughness dynamics is compatible with the standard Kardar–Parisi–Zhang (KPZ) or the quenched KPZ equations either in plain or methylcellulose (MC)-containing gel culture media, respectively. In both cases, the influence of a non-uniform distribution of the colony constituents was significant. These results encouraged us to investigate the overall dynamics of those systems considering the morphology and size, the duplication rate, and the motility of single cells. For this purpose, colonies with different cell populations (N) exhibiting quasi-circular and quasi-linear growth fronts in plain and MC-containing culture media are investigated. For small N, the average radial front velocity and its change with time depend on MC concentration. MC in the medium interferes with cell mitosis, contributes to the local enlargement of cells, and increases the distribution of spatio-temporal cell density heterogeneities. Colony spreading in MC-containing media proceeds under two main quenching effects, I and II; the former mainly depending on the culture medium composition and structure and the latter caused by the distribution of enlarged local cell domains. For large N, colony spreading occurs at constant velocity. The characteristics of cell motility, assessed by measuring their trajectories and the corresponding velocity field, reflect the effect of enlarged, slow-moving cells and the structure of the medium. Local average cell size distribution and individual cell motility data from plain and MC-containing media are qualitatively consistent with the predictions of both the extended cellular Potts models and the observed transition of the front roughness dynamics from a standard KPZ to a quenched KPZ. In this case, quenching

✉ M. A. Pasquale
miguelp@inifta.unlp.edu.ar

[1] Instituto de Investigaciones Fisicoquímicas Teóricas y Aplicadas (INIFTA), Universidad Nacional de La Plata (UNLP), CONICET, Sucursal 4, Casilla de Correo 16, 1900 La Plata, Argentina

[2] Cátedra de Patología, Facultad de Ciencias Médicas, UNLP, CIC, Calle 60 y 120, 1900 La Plata, Bs. As., Argentina

effects I and II cooperate and give rise to the quenched-KPZ equation. Seemingly, these results show a possible way of linking the cellular Potts models and the 2D colony front roughness dynamics.

Keywords Vero cell culture · Colony heterogeneities · Cell motility · Growth models · Dynamic scaling

1 Introduction

There are different procedures to interpret dynamic data associated with the study of complex mechanisms, such as those involved in the dynamics of living systems, which usually requires the analysis of physical, chemical, and biological concurrent processes, particularly when looking for either a rational understanding of nature or improved skills for handling the dynamics of biological phenomena. This is a matter of interest in processes involved in wound healing or malignant tumor growth [1, 2]. One of these procedures is based upon the dynamic scaling analysis (DSA) of colony fronts [3–12]. In this approach, the two-dimensional (2D) cell colony front dynamics is characterized through a set of dynamic scaling exponents (α, β, z, the roughness, the growth, and the dynamic exponents, respectively) derived from DSA applied to the colony front profiles and by comparing them with those expected from different complex statistical models [13, 14]. These approaches have provided data on non-Euclidean 2D spreading biological interfaces that were interpreted in terms of the standard Kardar, Parisi, and Zhang (KPZ) continuous equation [7, 8, 12, 15]. Later, this approach was used to investigate the cell colony dynamics in a gel medium that enhanced the appearance of heterogeneities [16]. Their influence has been ascribed to spatio-temporal-dependent interactions among either cells or cells with constituents of each culture medium that determine the characteristics of individual cell motility [17]. Accordingly, the dynamic scaling analysis of 2D colony front spreading in a gel medium yields a set of exponents comparable to those expected for quenched KPZ (QKPZ) dynamics [16].

Another approach to these complex mechanisms started from the behavior of individual cells as in cellular Potts models (CPMs) [18, 19] that were grounded on dynamic data derived from either individual or collective cells at different colony regions [18–21]. Accordingly, the description of these bio-systems comprised cell motility under chemotaxis with randomly fluctuating cell shapes and continuous deterministic equations related to cellular density distributions. In addition, from microscopic dynamics utilizing the excluded volume approach, non-linear diffusion equations with diffusion coefficients depending on cellular volume fraction to prevent the collapse of cellular density were obtained [20]. These versatile models have been applied for interpreting different aspects of cell physiology [20–28]. Thus, an extended CPM version provided a strong correlation of cell migration directionality with topological surrounding extracellular matrix (ECM) distribution and a biphasic dependence of migration on the matrix structure and stiffness, cell density, and adhesion [27]. In this case, the simulation of cell locomotion in highly constrained fibrillar obstacles required cell nucleus deformations and/or the activity of cell-derived proteolysis. Accordingly, cell motility was modulated by a spatio-temporal-dependent set of multilevel mechanisms that were influenced by both the biochemistry of extracellular and intracellular signaling. Cell motility was further modulated by a number of mechanisms in which relevant variables from both the ECM and the cell itself were included [29]. A cell-based model with a cellular Potts formalism describing spontaneously emerging, randomly oriented collective

cell streams within a human keratinocyte culture monolayer has also been reported [30]. In this model, by changing the relevance of mechanical links between cells, the experimental findings that cell streams become narrower with the decrease in cell–cell adhesion have been explained. A more recent CPM considered generalized cells mapped out on a uniform 2D Cartesian grid, cells being taken as extended objects composed of a collection of grids [28]. Its stochastic simulation included the effect of cell migration, compression, and contact inhibition to describe the evolution of cell size distribution and the global colony growth. Furthermore, a phase field cell monolayer model with its dynamics approaching the continuous limit of the Potts model has been used to describe the increase in the motility of cells softer than their neighbors, in agreement with experimental data from human metastatic breast carcinoma cells (MDA-MB-231) co-cultured with normal epithelial cells (MCF10A) [31]. In this case, carcinoma cells are softer than normal cells [32] and the mismatch in cell elasticity causes several speed "bursts" in which the cancer cell relaxes from a largely deformed shape and consequently, its translational motion increases. The above-mentioned shows that experimental colony dynamic data, from single cells to cell clusters, are of interest for interpreting the influence of spatio-temporal heterogeneities on the colony spreading mechanism [14], in which structural and dynamic characteristics of the medium interfere with molecular recognition-dependent functionalities [33].

In the present work, data on the 2D spreading of Vero cell colonies, the cell size and shape and the individual migration of cells in plain and methylcellulose (MC) containing media, the latter paying particular attention to the gel medium, are reported. For this purpose, Vero cell colonies with different initial cell populations (N), colony ages and spreading geometries in culture media containing different MC concentrations (c_{MC}) are studied. MC is a hydrophilic polymer used, for instance, in cell cultures to study viral replication processes [34, 35], which yields clear, non-adhesive, viscous solutions that thicken the medium [36]. MC is non-toxic for cells although it affects both the interfacial dynamics and the bulk configuration of the bio-system. A part of this research, concerning large colonies with quasi-linear fronts propagating in MC-containing gel medium, has been reported in a previous paper [16] where it was observed that the occurrence of quenching effects interfered with the 2D colony front dynamics.

This paper refers to new data from different colonies as mentioned above, allowing us to distinguish a set of processes at the cell scale to advance an explanation of MC-induced quenching effects that slow down the colony growth velocity and to hint at a microscopic explanation of the change in the front roughness dynamics. These quenching effects depend on several interrelated characteristics of the cell culture mainly associated with physicochemical characteristics of the medium, the colony cell population, the local average cell area ($<A>$) and shape, the spatio-temporal cell density distribution, and the colony front spreading geometry. Cell trajectories and biased cell velocity components appear to be influenced by quenching effects due to the presence of MC in the culture medium. The analysis of individual cell trajectory data and the velocity field in both the plain and the gel media provides information on the contribution of cell-biased displacements in their trajectory towards the colony front. Furthermore, cell mean square displacement (*msd*) data indicate that in plain and gel media cell displacements involve a ballistic contribution, although the *msd* magnitude in the plain medium is greater than in the gel medium. Changes in the directionality of cell trajectories and cell size distributions while going from the plain to gel media and the c_{MC}-dependent colony spreading kinetics are qualitatively compatible with the predictions of extended cellular Potts models and are useful to account for the appearance of a quenched noise term in the QKPZ equation. Thus, the comparison of colony front spreading and dynamic scaling analysis data, as well as changes in the local colony heterogeneities and cell motility characteristics in

the different media, suggest the occurrence of reliable links between global (DSA) and individual cell-based (CPMs) approaches for further understanding the dynamics of this bio-system.

2 Experimental

2.1 Colony preparation procedures

Vero cells (passages 165–180) were cultured in Roswell Park Memorial Institute (RPMI 1640) medium containing 10% fetal bovine serum (FBS) (henceforth plain medium), under 5% carbon dioxide atmosphere at 37 °C and 97% humidity. Cell viability was routinely checked employing the exclusion Trypan-Blue test. Cell proliferation was examined by nuclear cell proliferation antigen Ki-67 from Dako. Cultures were immunostained by the standard streptavidin-biotin-peroxidase method employing Dako Universal LSAB 2 kit/HRP.

Experiments were run utilizing either the plain medium or MC-containing media. The latter, either sol or gel, were made by mixing RPMI medium prepared at 2 × containing 20% FBS, aqueous 5% MC (Sigma Aldrich, approximate molecular weight 14,000, catalogue number M7027) solution (250 cps dynamic viscosity) and the appropriate amount of water. Then, the plain medium, 0.5% and 1.0% MC sol media, with 1.0, 2.0, and 4.6 cps dynamic viscosity, respectively, and the 2.5% MC gel medium with ca. 22.6 cps dynamic viscosity, were used.

Different procedures were utilized to prepare three types of colonies (I, II, and III). Colonies I and II rendered complementary colony spreading data on global processes occurring in type III colonies. Thus, type I colonies (low population and quasi-circular fronts) were useful to learn about the dynamic behavior of relatively low population colonies and the evaluation of 2D kinetic data at early stages of growth in different media. Type II colonies (large population and quasi-circular fronts) were utilized to study both morphological and dynamic aspects from colonies with a large population in the gel media. Data from these experiments allowed us to investigate how changes in the colony spatio-temporal heterogeneities due to both the cell size and shape affected the distribution of local cell clusters and the appearance of enlarged cells, i.e., cells of size considerably exceeding the average size of cells that initially formed the colony as shown in Figs. 1d, 2, and 3. These changes influence the dynamics of both the 2D colony/medium and the inner central three-dimensional cluster/2D colony interfacial regions. Type III colonies (quasi-linear fronts) involving large N (large population and quasi-linear fronts) displayed a quasi-linear spreading geometry at constant front length. They were employed for determining cell motility parameters, by either manual cell tracking or particle image velocimetry (PIV), to obtain further details about the influence of the spatio-temporal colony heterogeneities on both the local cell morphology and the colony spreading dynamics. The comparison of these data to those resulting from type II colonies allowed us to envisage the influence of the expanding colony geometry on the evolution of its morphology and spreading dynamics. Type II and III colonies showed consolidated 2D fronts and the formation of 3D cell clusters in the colony bulk.

Type I colonies were prepared in plain medium by shedding disaggregate cells (500–1000 cell ml^{-1}) in Petri dishes. After about 48 h, when the colony pattern exhibited the appearance of cell clusters, the plain medium was replaced by the MC-containing one. Usually, about 5–10 cell clusters from each Petri dish were selected to follow up their spreading in the new medium.

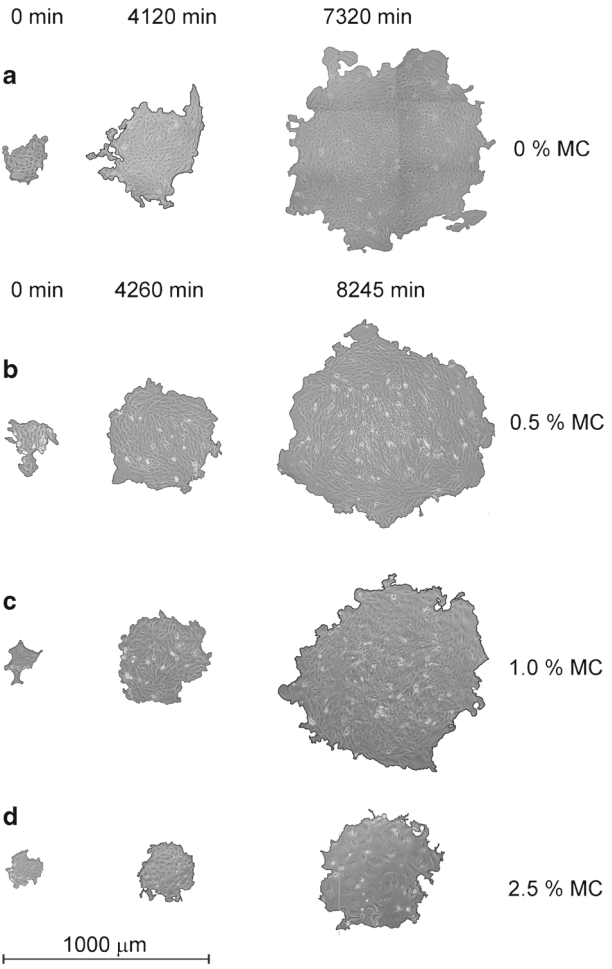

Fig. 1 Evolution of type I colony patterns in different culture media from $N_0 < 100$ cells. $N_0 = 50$ (**a**); 50 (**b**); 35 (**c**); and 90 (**d**) cells

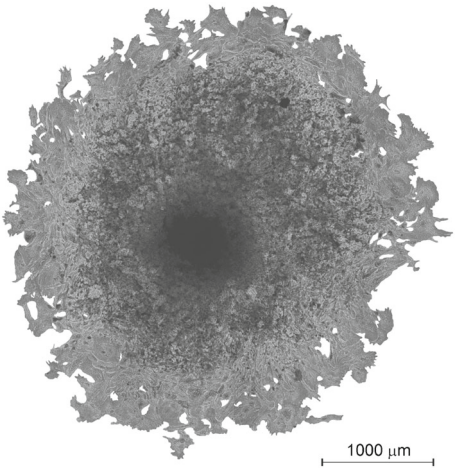

Fig. 2 Typical growth pattern of a type II colony grown up to $t = 16{,}000$ min in the gel medium ($c_{MC} = 2.5\%$). Three cell density pseudo-concentric regions can be distinguished: an outer 2D one with a number of holes, a central 3D core, and an intermediate region with a mixture of 2D and 3D cell domains

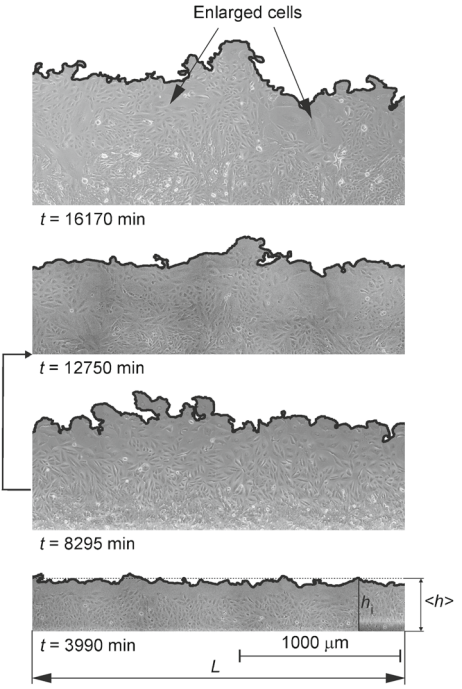

Fig. 3 Sequential images of front sections from a type III colony in the gel medium. The baseline from the image at $t = 8295$ min was shifted up at images for $t = 12\,750$ min and $t = 16\,170$ min to compensate for the colony width increase at the two upper images. *Arrows* indicate domains of enlarged cells at the colony border

Type II colonies were prepared by leaving a 2D colony to spread in plain medium until a 3D cluster of about 250–300 μm radius at the center of the colony was formed. The cluster was carefully transferred with a micropipette into a second Petri dish also containing plain medium and was left for 24 h. Subsequently, the medium was replaced by a MC-containing one and then the follow-up of the colony growth pattern began.

Type III colonies were prepared by first covering the central region of the Petri dish bottom with a 2.2-cm-wide and 100-μm-thick sterilized Teflon stripe [7]. Then, disaggregated cells (30,000–40,000 cell ml^{-1}) were seeded and left to grow for about 2 days until confluence in the Teflon-free region was reached. The Teflon stripe was removed, leaving a cell-free central region with the formation of two facing linear colony fronts of length L and eventually the plain medium was replaced by the MC-containing one. Afterwards, the colony was left to grow in opposite directions perpendicular to L. From this stage on ($t = t_0$), the colony pattern and the 2D front displacement were followed up.

2.2 Analysis of colony patterns

Sequential images of colony patterns were recorded utilizing a Nikon model DS-Fi1-U2 digital camera coupled to a Nikon TS100 phase-contrast inverted microscope with a CFI flat field ADL 10X objective at a resolution of 0.88 μm/pixel. Colony fronts were manually traced from computer screen images using a Wacom graphic tablet with a trace error on the order of the pixel. The follow-up of colony growth patterns was extended for about 12 days, a time at which a collapse of the colony front with some isolated free cell cluster in the Petri dish surface became possible.

In situ type III colony growth experiments were performed by placing each growing colony in a Petri dish inside a chamber fixed to the microscope platform. This chamber was kept under a controlled environment at 37 °C, 97% humidity, and culture medium pH = 7.4, the latter being preserved by employing the L-glutamine supplemented CO_2-independent (Gibco, Invitrogen Corp.) medium with and without MC. Colony front patterns from in situ experiments were recorded over 2–3 days by a time-lapse procedure at intervals in the range $5 \leq \Delta t' \leq 45$ min.

Both the cell morphology and the cell size distribution in colony types II and III were determined from sequential colony pattern images after fixing and staining with May-Grünwald-Giemsa. Cell contours were hand-traced as described above and their geometric features were determined by in-lab routines.

2.3 Evaluation of cell displacements

Trajectories of individual cells within colonies were evaluated from their instantaneous *x*-*y* coordinates ($\mathbf{P}_j = \mathbf{p}(t_i) = x_j(t_i), y_j(t_i)$, i = 1, 2,…*n*) by manually tracking time-lapse movie frames employing Image Pro Plus 6.0 software (Media Cybernetics, Inc.). Position coordinates from either the cell nucleus or the centroid of each cell contour were evaluated. The difference between those procedures, evaluated by averaging ten trajectories for about 24 h, was about 10%.

The mean cell velocity $<V_i>$ was obtained from coordinate data according to:

$$\langle V_i \rangle = \frac{\mathbf{p}_j(t_{i+1}) - \mathbf{p}_j(t_i)}{\Delta t'}. \tag{1}$$

The velocity components parallel (V_x) and perpendicular (V_y) to the colony front were evaluated within the $15 \leq \Delta t' \leq 45$ min interval. On the other hand, the mean square displacement resulted from:

$$msd = \left\langle \left((x_i(t_0 + \Delta t) - x_i(t_0))^2 \right) + \left((y_i(t_0 + \Delta t) - y_i(t_0))^2 \right) \right\rangle \tag{2}$$

where t_0 and Δt are the starting time and the recording interval, respectively. Average cell trajectory data from all values of t_0 were derived according to references [37, 38].

The *msd* dependence on Δt can be expressed by the power law:

$$\langle msd(\Delta t) \rangle \propto \Delta t^b \tag{3}$$

where the limiting values of constant *b* are 1 for random walk displacement and 2 for ballistic motion [37].

Cell tracking was carried out within a 720–4320-min interval. Only cells located within a border region width equivalent to three average cell diameters were tracked.

Cell motility was also studied by particle image velocimetry [39] using PIVlab 1.35 software [40] of MATLAB (The MathWorks, Natick, MA). Image sequences recorded for 255 min with $\Delta t'$ = 15 min were filtered and analyzed with an interrogation window of 82 × 82 pixels with 50% overlap. This technique was used to evaluate the angle formed by the velocity vector with respect to the baseline of type III colonies.

3 Results

3.1 Morphological changes

3.1.1 Type I colonies (low population and quasi-circular fronts)

Type I colony patterns starting from $N_0 < 100$ cells in different culture media (Fig. 1) show that, initially, irregular colony borders tend to approach a quasi-circular figure as the colony grows. In the range $0 \leq t \leq 9000$ min, the process is accompanied by a gradual decrease in the average cell–cell distance in the bulk yielding slightly more compact cell domains. The reverse effect is observed at the border region where cells of sizes larger than those of regular cells are formed. These changes are enhanced as c_{MC} in the medium increases and become more remarkable in the gel medium where the earlier appearance of enlarged cells, either at the colony border or inner regions, begins to be observed. The influence of c_{MC} on the increase of the average cell size in different regions of the colony is concurrent with an inhibition effect of MC on cell mitosis, as described further on and an enhancement in the colony front roughness with the appearance of horn-like protrusions and voids in between. Accordingly, the composition of the culture medium contributes to generating spatio-temporal heterogeneities that play a key role in the dynamics of these bio-systems.

3.1.2 Type II colonies (large population and quasi-circular fronts)

Type II colonies, particularly in the gel medium, show a fast appearance of enlarged cells at the colony border. They produce a remarkable decrease in cell density and an increase of the spatio-temporal heterogeneity in these colonies due to the occurrence of different local cell density domains. Thus, for $t = 16{,}500$ min (Fig. 2) the 2D colony border region consists of regular cells, enlarged cells and small voids. Enlarged cells form a sort of barrier at the colony outer ring that perturbs the displacement of smaller cells moving outwards. The innermost region of these colonies shows a central 3D phase surrounded by a rather compact 2D intermediate layer of regular cells limited by the low density border region. At this growth stage, the colony front becomes considerably rough due to the formation of voids and protrusions, some of them displaying small horn-like shapes. Likely, voids at the 2D region favor cell motion towards the colony front.

3.1.3 Type III colonies (large population and quasi-linear fronts)

Growth patterns of these colonies in the gel medium show that the average front morphology remains almost unchanged up to about 5000 min. Later, the progressive formation of enlarged, slow-moving cells and domains of small polarized ones are observed (Fig. 3). As for type II colonies, enlarged cells are mostly located at the colony front, their average size increasing with the colony age. Thus, the average cell diameter changes from about 45 μm at $t = 2400$ min to about 250 μm at $t = 19{,}620$ min, i.e., a value fourfold greater than those found for the largest cells in the plain medium [7].

A more detailed observation of these patterns confirms that domains of enlarged cells behave like slow-moving obstacles hindering the advance of smaller neighboring cells towards the colony front. As discussed further on, these obstacles, play a key role in the distribution of individual cell velocity components in their trajectory towards the colony front.

The comparison between in situ time-lapsed sequential growth patterns in plain and gel media allowed us to envisage the influence of individual cell dynamics on the characteristics of quasi-linear colony front roughness. To observe the changes produced in the colonies, at both relatively early and late growth stages after colony full adaptation to the new medium, the follow-up of sequential growth patterns was started at different times after removing the Teflon stripe from the Petri dish. Colony patterns recorded at early stages in the plain medium exhibit minor changes in both the average shape and size of cells, in contrast to those ones from the gel medium (Fig. 4). For the latter, a preferred orientation of polarized cells towards the colony front and a local front roughness increase are observed. On the other hand, in the gel medium, sequential images of colony morphology patterns at advanced stages of growth (Fig. 5) show that the average size of enlarged cells at the colony border further increases and that they are partially surrounded by small regular cells. In the plain medium, the number and the average size of enlarged cells are smaller than in the gel medium.

3.2 The average area of cells at different colony regions

The local average size of cells was determined at different regions of type II and III colonies. For type II colonies, comparative histograms, obtained at two 200 μm wide colony stripes from the borderline inwards, show that the average cell area decreases when going towards the colony center (Fig. 6). For the outer stripe, the average cell area is larger than about 500 μm^2. These results are consistent with the morphology patterns described above (Fig. 2), in which a rather compact barrier of enlarged cells at the colony front is formed.

For type III colonies, in both plain and gel media, cell area histograms were calculated by selecting a rectangular 2000 μm long and 600 μm wide colony front region parallel to the front, subdivided into three stripes of 200 μm width each (Fig. 7). These results show that in the plain medium at the outer colony region, cells with an average area below 400 μm^2 prevail and between 400–600 μm depth, the average cell area is below 120 μm^2. In the gel medium, a relatively greater contribution of enlarged cells is observed. In this case, the histogram corresponding to the outer 0–200 μm stripe displays two maxima at ca. 100 μm^2 and ca. 550 μm^2, whereas at the innermost part of the colony, the contribution of enlarged cells decreases, although it always remains greater than in the plain medium.

3.3 Colony spreading kinetics

Type I colonies with N_0 about 100 cells growing in a medium containing $0 \le c_{MC} \le 1\%$ show a cell population rate that follows first-order kinetics over the range $0 < t < 9000$ min (Fig. 8a), with a c_{MC}-dependent average velocity constant $\langle k_N \rangle$ being the reciprocal of an average cell duplication time ($\langle \tau \rangle$), i.e., $\langle k_N^{-1} \rangle = \langle \tau \rangle$. Unfortunately, for $t > 11{,}000$ min, the appearance of new regular cells, 3D cell domains in the colony bulk and enlarged cells at the colony border region render individual cell counting uncertain.

On the other hand, the radial colony spreading kinetics expressed in terms of the average radius displacement also fulfils an exponential law up to ca. 9000 min with an average kinetic constant $\langle k_R \rangle$ (Fig. 8b). For both plain and sol media, the value of $\langle k_N \rangle$ is about twice that of $\langle k_R \rangle$, as expected [8]. It is worth noting that for sol MC-containing media, the $(\langle k_N \rangle)/(\langle k_R \rangle)$ ratio is similar to that resulting from the plain medium but it decays abruptly in the gel medium. Moreover, for the latter, within the 3000–10,000-min range (Fig. 8c) data from both the $\langle R/R_0 \rangle$ and the average square root of normalized cell areas $(\langle A_{cell}/A_{cell,0} \rangle)^{1/2}$ fall on the

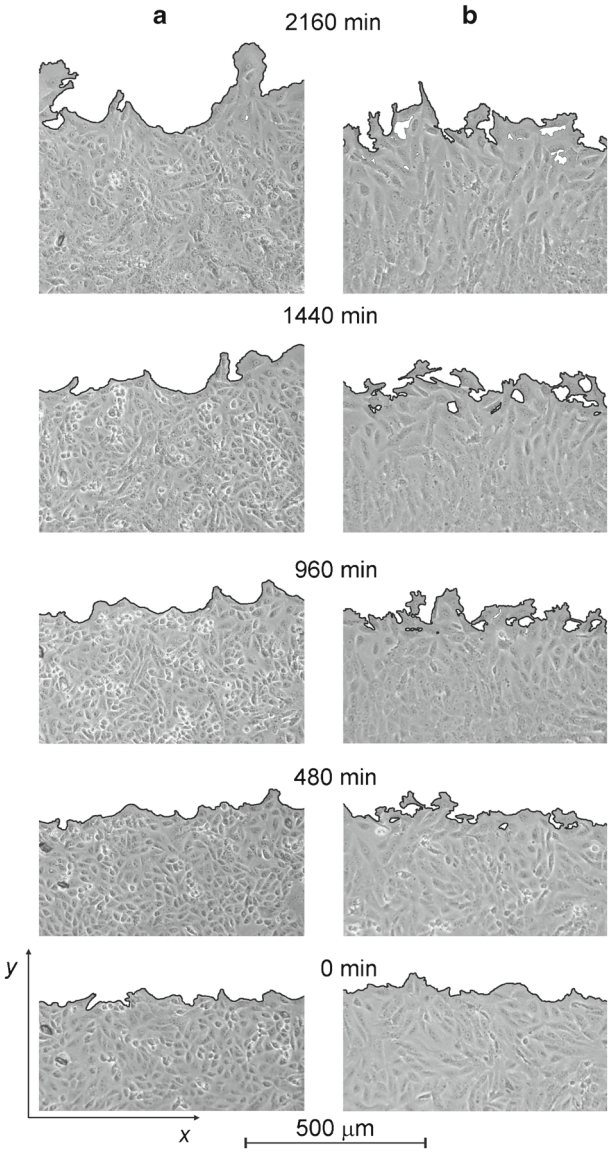

Fig. 4 Comparison of two front sections from sequential growth patterns of type III colony in the plain medium (**a**) and the gel medium (**b**). In situ image sequences started 9 h after removing the Teflon stripe from the Petri dish

same curve. This fact indicates that the colony front displacement is mainly governed by the increase in the average cell area.

Data displayed in Fig. 8b show that the greater c_{MC}, the shorter the range of t where the exponential kinetics is fulfilled. In the sol medium, the value of $\langle k_N \rangle$ decreases slightly with c_{MC}, in contrast with the abrupt drop observed in the gel medium. Conversely, $\langle k_R \rangle$ slightly decreases with c_{MC} (Table 1).

These results are consistent with a colony front displacement under increasing quenching effects as c_{MC} increases. On the other hand, the slope of the $\langle R/R_0 \rangle$ versus t plots at $t = 3500$ min (S_{3500}) follows a linear relationship with the reciprocal of the dynamic viscosity

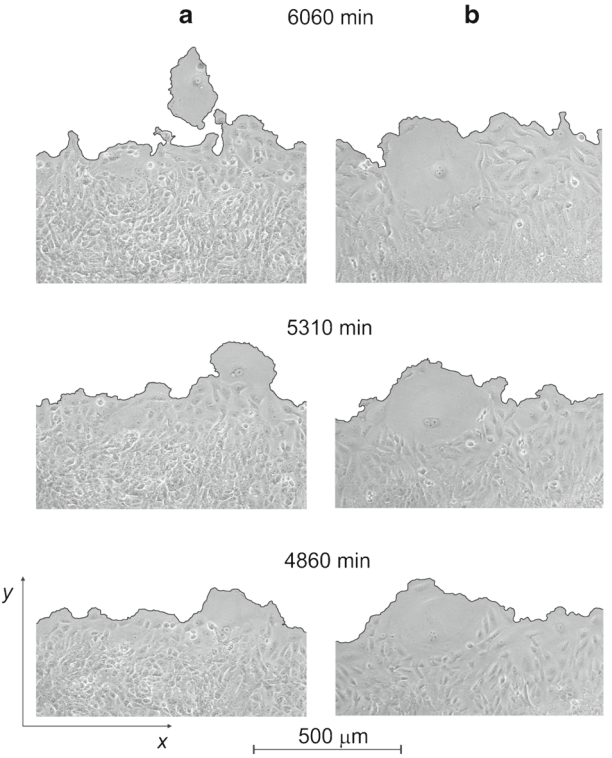

Fig. 5 Comparison of two front sections from sequential growth patterns of type III colony in the plain (**a**) and the gel medium (**b**). In situ sequential imaging started 80 h after removing the Teflon stripe from the Petri dish

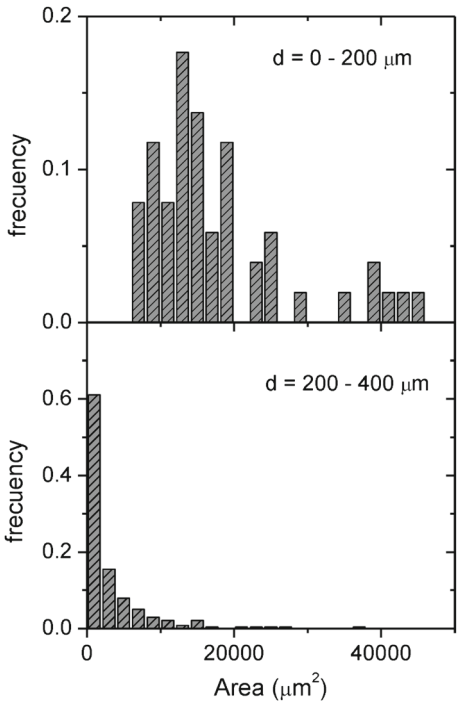

Fig. 6 Average cell area histograms from a type II colony in 2.5% MC for t = 19,000 min at two adjacent colony regions d = 200 μm in width, selected from the colony border inwards

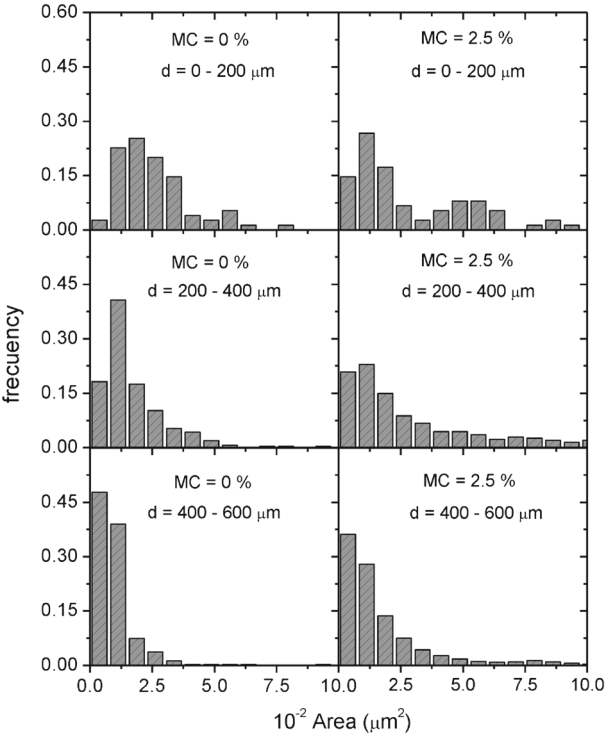

Fig. 7 Comparative average cell area histograms from 200-μm-wide stripe regions of type III colonies at t = 7200 min in the plain and gel media

(η^{-1}) (Fig. 9). It should be noted that at t = 3500 min, colonies exhibit an almost constant average cell size and spreading occurs under exponential kinetics with a negligible influence of enlarged cells. Under these circumstances, the decrease of $\langle k_R \rangle$ with c_{MC} is mostly determined by the structure and hydrodynamic properties of the culture medium.

Type II colonies, with large N growing in the gel medium beyond 20,000 min, were first grown for 1000 min in the plain medium, which was then replaced by the gel medium, where colony growth continued. In the gel medium, the $\langle R \rangle$ versus t plot exhibits two reasonable straight lines, a first one for $t < 6000$ min with a slope of ca. 0.090 ± 0.005 μm min^{-1} and a second one from $t = 6000$ min upwards with a slope of 0.064 ± 0.005 μm min^{-1} (Fig. 10). This change is associated with the formation of the barrier of enlarged cells at the colony front that restrains the spreading rate. This effect, coupled to specific physicochemical properties of the medium, results in a cooperative retarding effect on the dynamics of the bio-system. Furthermore, it should be noted that the radial expansion of the central 3D cell cluster also follows a linear relationship with the slope of 0.055 ± 0.005 μm min^{-1} for $t > 6000$ min, approaching the kinetic behavior of the colony border. This coincidence suggests that the colony spreading involves cell displacements from the inner regions to the border of the colony, through an almost constant effective 2D outer layer built up by a growth process under the influence of cooperative quenching effects.

For the type III colony in the plain medium, a constant velocity $v_F = 0.220 \pm 0.003$ μm min^{-1} is obtained (Fig. 11a), a figure that decreases to 0.126 ± 0.003 for the gel medium (Fig. 11b).

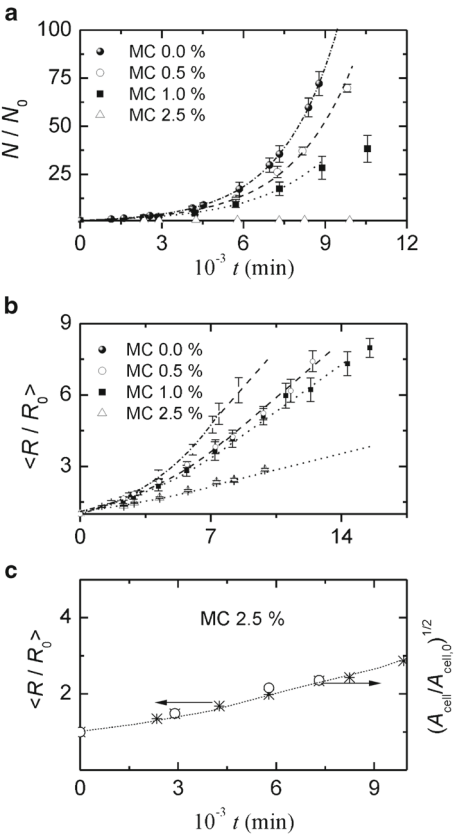

Fig. 8 Normalized kinetic data from type I colonies in different culture media. **a** Average cell population; **b** average radius; **c** square root of average cell area. R_0 and N_0 are the initial colony radius and cell population, respectively. Standard error bars are indicated

3.4 Cell duplication rate

Cell mitosis plays a significant role in spatio-temporal changes accompanying the colony 2D spreading in both the plain and gel media, as demonstrated by Ki-67 staining of cell cultures. Stained colony patterns from the plain medium exhibit a large number of cells under duplication and a very scarce number of enlarged cells (Fig. 12a), while colony patterns in the gel medium show only a few small clusters of stained (i.e., duplicating) cells (Fig. 12b) and enlarged cells that appear inactive for duplication. Consequently, the inhibition in cell mitosis (proliferation) shown by immunostaining is consistent with the decrease in $\langle k_N \rangle$ as c_{MC} increases.

Table 1 First-order kinetic constants $\langle k_N \rangle$ and $\langle k_R \rangle$ for type I colonies for different MC concentrations

c_{MC}	$10^4 \langle k_N \rangle$	$10^4 \langle k_R \rangle$
0.0	4.9 ± 0.3	2.2 ± 0.1
0.5	4.4 ± 0.3	1.60 ± 0.05
1.0	3.9 ± 0.3	1.50 ± 0.05
2.5	→0	0.95 ± 0.05

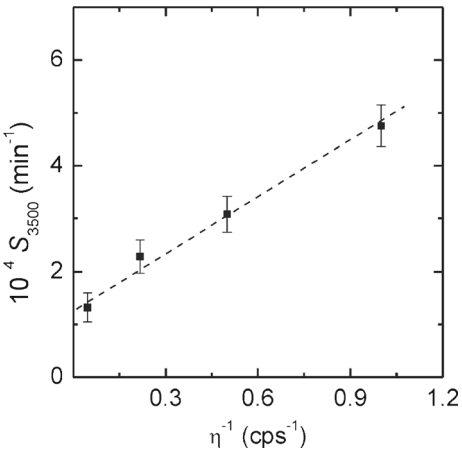

Fig. 9 S_{3500}, the slope $d<R/R_0>/dt$ at $t = 3500$ min taken from (Fig. 8b), versus the reciprocal of the dynamic viscosity (η^{-1}) of the culture medium. Type I colonies in different culture media within the range $0 \leq c_{MC} \leq 2.5\%$ are included

3.5 Cell motility in type III colonies

Individual cell trajectories were tracked from runs made with type III colonies in both plain and gel media, as these colonies provided the most adequate configuration for evaluating parallel and perpendicular components of velocity vectors with the techniques used in this work.

Tracking diagrams of individual cell trajectories in the plain medium tend to become random at inner regions of the colony and exhibit a greater directionality at outer regions. This difference should be related to the asymmetry of the collective cell displacements in the colony accompanying the motion of individual cells (Fig. 13a, b) guided by colony spatio-temporal heterogeneities. The colony exhibits distinguishable distributions of cell density domains in the colony and the occurrence of protrusions at the border. In the gel medium, biased displacements of individual cells are more clearly observed as the contribution of collective movements diminishes (Fig. 13c, d). Likewise, trajectory diagrams of cells located

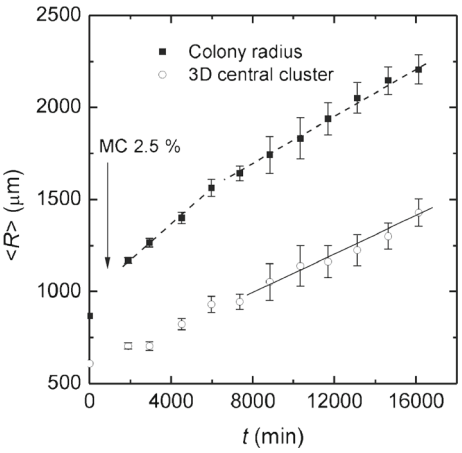

Fig. 10 Dependence of the average colony radius and central 3D average cell cluster radius on growth time for type II colonies. The *arrow* indicates the time at which the plain culture medium was replaced by the gel medium

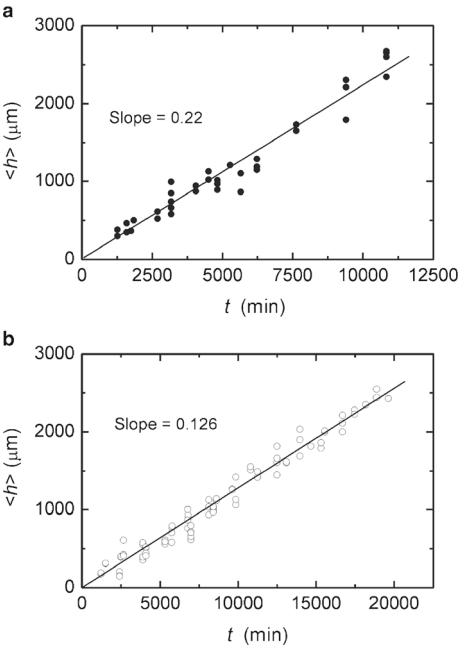

Fig. 11 Average colony front displacement versus colony spreading time from type III colonies. **a** Plain medium; **b** gel medium. Scattering data correspond to different runs

at colony front regions in the presence of enlarged cells show trajectories of smaller cells moving towards the front circumventing those cells (Fig. 13e, f). In addition, histograms related to the perpendicular velocity component display two maxima that are consistent with two predominant cell populations with characteristic motilities. Therefore, the presence of enlarged cells at border regions imposes atypical velocity components on individual trajectories of regular cells.

The fact that cell motility in the gel medium is slower than in the plain medium confirms the influence of the rheological characteristics of the medium on the average individual cell

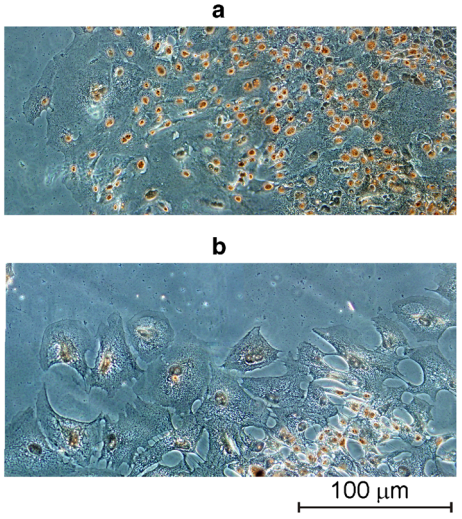

Fig. 12 Ki-67 staining of Vero cells at the front region of colonies grown for $t = 7200$ min in plain (**a**) and gel media (**b**)

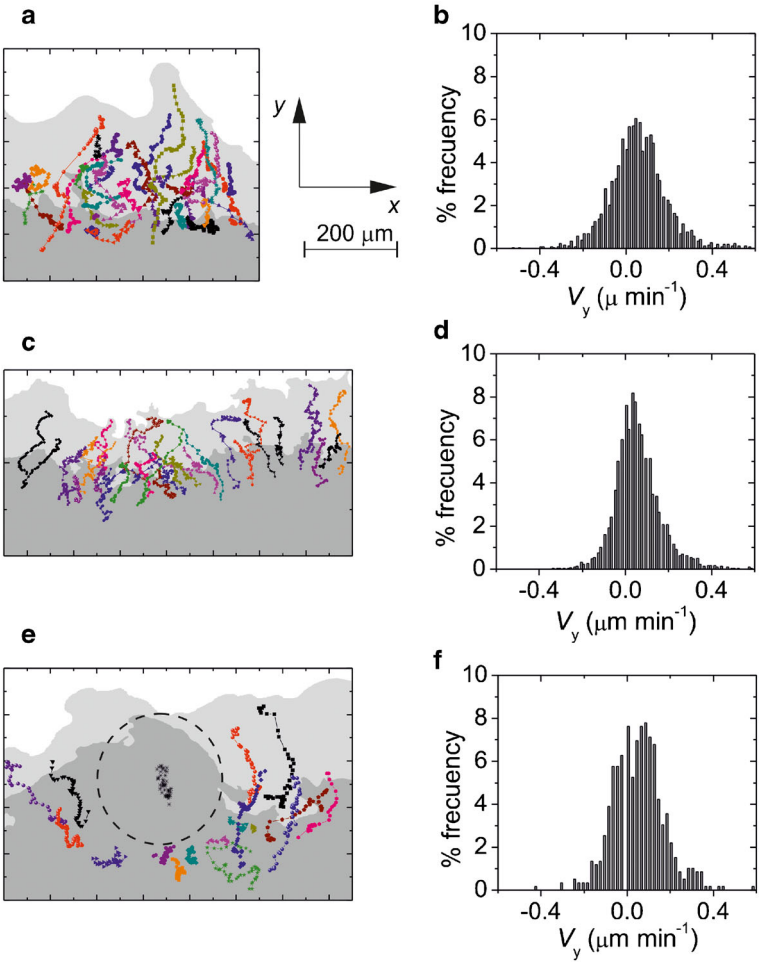

Fig. 13 Individual cell trajectories and y-velocity component histograms of the cell trajectories with $\Delta t' = 30$ min from a type III colony in: (**a**, **b**) plain and (**c**, **d** and **e**, **f**) gel media. Their follow-up started at $t = 1050$ min (**a**, **b**), 540 min (**c**, **d**), and 4800 min (**e**, **f**)

velocity. The *msd* versus *t* log-log plots exhibit a linear relationship for both media but the average *msd* values at each time interval decrease when going from the plain to the gel medium (Fig. 14), suggesting that individual cell motility also diminishes, in agreement with V_y histograms. For the shortest time intervals, the slope of the linear relationship is 1.46 ± 0.04 for the gel medium and 1.65 ± 0.04 for the plain medium. These slopes, ranging between 1 and 2, are consistent with the relative contributions of the *x* and *y* biased components to individual cell trajectories.

On the other hand, velocity field images of individual cells from both plain and gel media were evaluated from PIV data. For this purpose, the colony field was divided into two 2D regions of about 600-μm width selected at the bulk and at the outermost part of the colony, respectively (Fig. 15). In the gel medium, as *t* increases, velocity vectors contained within the former region are mainly oriented towards the colony front displacement direction. The

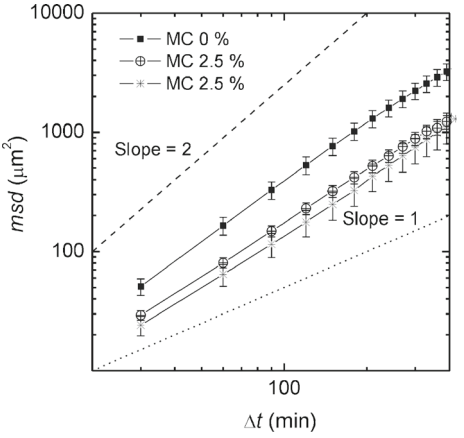

Fig. 14 Average mean square displacement of individual cells at the colony border region versus time. Data from type III colonies in plain medium with t_0 = 1050 min (*black squares*), in gel with t_0 = 540 min (*open circles*) and in gel medium with t_0 = 4800 min (*stars*). For the sake of comparison, lines corresponding to a random walk displacement (slope = 1) and a ballistic motion (slope = 2) are also plotted

comparison of the evolution of histograms in terms of the angle formed by the velocity vector with respect to the baseline of colony spreading (Fig. 16) reveals that for the gel medium, as the colony age increases, the vector angle in the bulk region also increases, whereas the vector angle at the outermost part of the colony decreases. These results indicate that while cells in the bulk tend to move in a rather preferential direction, those at the border move more randomly as their vector angles are outside the 45–135 degree range.

3.6 Dynamic scaling analysis

According to dynamic scaling analysis [3], the interface roughness ($w = \sum_{(i=1\rightarrow L)} [h(i,t)- <h(t)>)]/L$, with $h(i,t)$ the colony front width at point i and $<h(t)>$ the average colony front width at t) of a 2D condensed system of size L, is expected to increase with time for $t << t_s$ (t_s denotes the roughness saturation time):

$$w \propto t^{\beta} \quad t << t_s \tag{4}$$

and when $t > t_s$, the roughness saturation w_s is attained. The latter should increase with L according to:

$$w_s \propto L^{\alpha} \quad t >> t_s \tag{5}$$

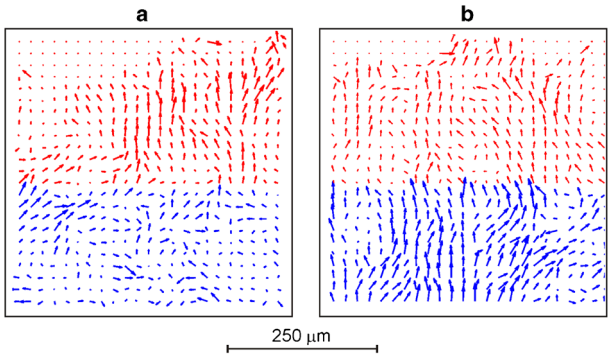

Fig. 15 Typical overlay of PIV velocity field images from type III colonies in the gel medium at t = 540 min (**a**) and t = 4800 min (**b**) after removing the Teflon stripe from the Petri dish. *Blue* and *red vectors* indicate cell trajectories in the bulk and in the border regions of the colony, respectively

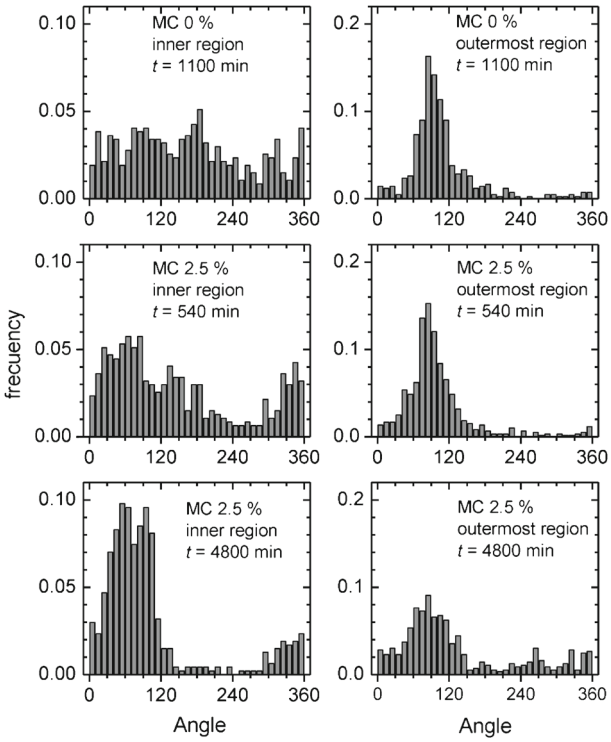

Fig. 16 Velocity vector angle histograms of cells from type III linear colonies in the plain and gel media evaluated at different colony regions and spreading times

where the value of t_s depends on the system size ($t_s \propto L^z$, $z = \alpha/\beta$) [3]. Therefore, from the slopes of the log $w(L,t)$ versus log t plot, one can evaluate the growth and roughness exponents β and α, respectively, and, from their ratio, the dynamic exponent z.

For a set of exponents the fulfillment of the Family-Vicsek scaling relationship is expected:

$$\frac{w(L,t)}{L^{\alpha}} \propto f\left(\frac{t}{L^{Z}}\right) \tag{6}$$

f being the scaling function.

Roughness data at different t were plotted according to Eq. (6) (Fig. 17a, b) for a set of colonies growing in plain and gel media (shown in Figs. 3, 4, and 5). A relatively good collapse was obtained with $\alpha = 0.50$ and $z = 1.5$ for colonies in the plain medium and $\alpha = 0.63$ and $z = 0.81$ for colonies in the gel medium. From the slopes, values of $\beta = 0.33$, and 0.75 for plain and gel media, respectively, were obtained.

4 Discussion

4.1 Influence of spatio-temporal heterogeneities on the 2D spreading colony dynamics

The morphology evolution of Vero cell colonies in the different media reveals that spatio-temporal heterogeneities manifested at both the cell and the colony levels. They are associated

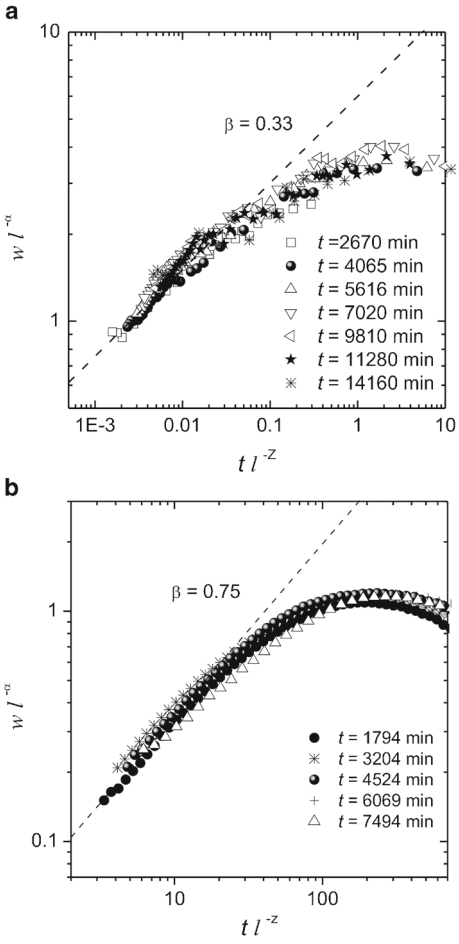

Fig. 17 Log-log plots of the Family-Vicsek scaling relationship from colony contour roughness data of type III colonies in plain medium (**a**) and gel medium (**b**)

with cell density, cell size distributions, as well as with changes in the physicochemical properties of the culture medium, their relative participation depending on colony type and age.

4.1.1 Type I colony

Type I colonies growing in plain medium from an initial quasi-homogeneous cell population remain almost constant in terms of average cell size and average local cell density when N is low (Fig. 1). As N increases, the colony heterogeneity plays an increasingly key role in the spreading kinetics. This is clearly manifested by the fact that the spreading kinetic transition from exponential to constant $<v_F>$ becomes more remarkable as one goes from the plain/sol to the gel media (Fig. 8). Accordingly, for type I colonies with low N, the direct relation between k_N and k_R (Table 1) indicates that the main driving force assisting the 2D spreading is cell duplication, which is progressively inhibited as c_{MC} increases. In the gel medium where $k_N << k_R$, the colony spreading is largely determined by the increase in the cell average size and the rheological properties of the medium.

As c_{MC} increases, the kinetic transition from exponential to constant $<v_F>$ occurs at shorter times and enlarged cells at the colony border begin to appear at the end of the exponential kinetic regime. At this stage, the colony morphology can be described in terms of an inner high-density region with a 3D phase consisting in packed small cells surrounded by a 2D outer ring involving small and enlarged cells. Small cells at the outer ring preferentially undergo duplication and displacements, mainly contributing to the colony expansion at constant $<v_F>$ (Figs. 1, 8, 10, and 11).

Colony spreading data from the plain medium are consistent with theoretical approaches that have been proposed to describe the growth of in vitro cell aggregates [41]. In those models, contact inhibition sets in as the local cell density exceeds a certain critical value. Seemingly, this inhibition is caused by mechanical interactions and constraints that define cell phenotypes unable to undergo mitosis or crawl [42]. The increased colony heterogeneity in the gel medium makes the application of these models difficult.

The foregoing discussion points out that driving forces in the 2D colony spreading are partially counterbalanced by retarding effects due to the spatio-temporal heterogeneities generated by the culture media interacting with the cells, affecting their morphology and phenotypes (mitosis time, motility characteristics, etc.) in the colony where they are physically and functionally connected during their displacements [43]. Depending upon the colony age, two main quenching effects can be distinguished, namely quenching effect I, which emerges at relatively short growth times and is likely linked to the medium's complex structure and quenching effect II, which is clearly seen at long growth times, particularly through the occurrence of enlarged cells. Quenching effect II is enhanced for colonies of type II and III, as referred to further on.

Quenching effect I results from the physical characteristics of MC-containing culture media (Fig. 12). MC with an intermediate degree of substitution of OH by methoxy groups in cellulose presumably yields a "cage-like" structure surrounding those hydrophobic methoxy groups that increases from sol to gel [36, 44, 45]. The structure of this gel network has been described as hydrophobic associated domains via bridge connecting junctions [46]. Quenching effect I should increase the friction coefficients linked to 2D cell displacements and deformations. This is consistent with the reciprocal linear relationship between the growth front displacement velocity and the dynamic viscosity (Fig. 9).

4.1.2 Type II colony

For type II colonies in the gel medium, enlarged cells build up a sort of barrier that perturbs the motility of regular cells towards the colony front (Figs. 2 and 6). These enlarged cells are characterized by their slow motility and low value of k_N (Figs. 12 and 13). From a physical standpoint, they behave like quasi-fixed obstacles compelling regular cells to find longer, strongly biased trajectories towards the front (Figs. 13, 14, 15, and 16). Quenching effect II is mainly related to the appearance of enlarged cells (Figs. 2 and 6) that progressively slow down the 2D colony front spreading. The $<v_F>$ values resulting from either the average 2D colony phase medium or the 2D/3D colony interfacial displacement tend to become similar (Fig. 10). For this type of colony, the transport of cells throughout inner 2D colony regions towards the colony front is assisted by a number of voids and channels already present in the colony, together with those free sites preceding the cytokinesis. In this case, it would also be possible that a small number of cells, coming down from 3D domains to interact with the substrate, participate in the spreading process. Consequently, the constant $<v_F>$ kinetic regime results

from a constant average cell density gradient driving force acting on individual cells moving through a 2D colony effective ring of quasi-constant average radial length.

4.1.3 Type III colony

For type III colonies, enlarged cells at the border region behave similarly to those described for type II colonies, except that in this case they display a rather discontinuous layer of enlarged cells as obstacles with relatively small free spaces in between. For type III colonies growing in both the plain and the MC-containing media (Figs. 3 and 5), the cell size histograms at relatively long age exhibit two maxima (Fig. 7). This feature becomes more remarkable for the gel medium where cell motility becomes slower than in the plain medium (Fig. 13).

Cell trajectory and PIV data show that enlarged cells, particularly at the colony front region, produce a significant bias in regular cell displacements in the direction parallel to the front (Figs. 13, 15, and 16). As regular cells move towards the colony front, they tend to acquire an elongated shape (Figs. 3, 4 and 5) due to local space restrictions. The average cell velocity and individual cell trajectories are considerably influenced by the spatio-temporal changes in cell shape and size, i.e., the local cell density distribution in the colony and by the composition and properties of the culture media. Cell motility data confirm that the magnitude of cell velocities and their local orientation are influenced by relatively large friction forces generated in the gel medium and different heterogeneities. The latter are generated by the presence of slow-moving, enlarged cells that produce biased cell trajectories and by the deformation of the gel medium in the direction of the colony front displacement, which becomes evident at inner parts of the colonies (Figs. 4, 5, 13, 15, and 16).

4.2 Cell-based models describing experimental data

CPM cell-based models consider that individual biophysical and molecular interactions between cells contribute to the free energy of the entire system. The latter is evaluated at every step of the system's evolution for determining the occurrence probability of a global process. In the extended CPM reported in [28], the cell duplication cycle, contact inhibition and the contributions of cell–cell and cell–medium interactions, medium properties, changes in free energy associated with cell shape and size, as well as the energetics of motility, were considered. Simulation results indicated that the interplay between cell stiffness and motility in cell shape and size causes cell compression. When the latter was constant, high cell motility involved tapered cells and a relatively fast colony growth. The larger the available space for cells, the larger their size. Thus, when cell compression was low and the motility restricted, as in the case of cells at the colony border region or for cells growing at low density, a bimodal cell size distribution was observed. This theoretical framework is qualitatively consistent with experimental data presented here (Figs. 7, 8, and 13). In the gel medium, cell motility is hindered and at the border region, MC macromolecules diminish cell–cell interactions and the cell size histogram shows two maxima.

Cell trajectory characteristics are at least qualitatively consistent with the extended Potts model predictions [27], in which the directionality of cell movements is a direct result of well-defined directional cues provided by specific matrices. The anisotropy of the matrices induces a reorientation of moving cells in the direction of the matrix threads and the consequent motion along them and, in comparison with isotropic matrices, generates a highly oriented locomotion. The model has similar velocities for cell motion either in isotropic or anisotropic matrices

but with an increase in persistence for the latter. It is worth noting that the model proposed in [27] considered only isolated cells interacting with the environment, whereas the model proposed in [30] included a cellular Potts formalism describing collective cell streams in epithelial monolayers [47]. In this case, it was concluded that intercellular adhesion modulated the extent of cell groups undergoing local collective movements in the monolayer. The disruption of cell adhesion complexes diminished the width of the streams. This explanation appears to be applicable to the disorder in individual cell motion and to the increase in the local front roughness of colony growth in the gel medium, even in the absence of enlarged cells (Figs. 4, 13b and 16). The MC structure interacts with the cell membrane [48], diminishing cell–cell interactions at the colony edge where they are rather smaller than at inner colony regions.

The preceding analysis reveals that spatio-temporal heterogeneities affect processes at both the colony and the cell levels and suggests the possibility of linking individual cell motility characteristics to the entire colony spreading interfacial 2D dynamics. The latter is characterized by the front roughness development in which a number of cell transport processes are involved. This matter is of interest in foreseeing possible stability conditions of biological interfaces. This approach has been considered in the multiscale models [20, 21] in which continuous non-linear transport equations have been derived from microscopic cell level properties, tackled by the CPM formalism.

4.3 Roughness dynamics of 2D fronts of Vero cell colonies

Dynamic scaling analysis was applied to type III colony fronts in both the plain and gel media as shown in Fig. 17a, b. These results confirm and complement those recently reported [7, 16]. The overall data indicate that for the plain medium, within the range $1400 < t < 10{,}000$ min and the front length range $150 < l < 15{,}000$ μm, the set of exponents from DSA is $\alpha = 0.50 \pm 0.05$ and $\beta = 0.32 \pm 0.04$, which is consistent with the prediction of the standard KPZ model, i.e., $\alpha = 0.50$, $\beta = 0.33$ and $z = 1.5$ [49]. Conversely, from those colonies in the gel medium, within the ranges $5000 < t < 10{,}000$ min and $200 < l < 20\,000$ μm, the set of exponents results in $\alpha = 0.63 \pm 0.04$, $\beta = 0.78 \pm 0.05$ and $z = 0.80 \pm 0.05$, in agreement with the prediction of a quenched-KPZ model, i.e., $\alpha = 0.63$, $\beta = 0.90$ [49, 50], which describes the motion of a condensed interface in a disordered medium by the equation:

$$\frac{\partial h}{\partial t} = \nu \nabla^2 h + \frac{\lambda}{2}(\nabla h)^2 + F + \eta(\mathrm{x}, h) \tag{7}$$

where the first rhs term accounts for the relaxation of the interface caused by a surface tension contribution, the second one considers the lateral growth that breaks the up-down symmetry and the third is the driving force F, which in this case is mainly related to cell proliferation and the average cell size increase in the colony. Finally, the term η(x, h) represents the quenched noise that is responsible for the increase in the local front roughness and overall colony growth dynamics [3, 50, 51].

Dynamic data from the gel medium reveal the contribution of multiple effects on the colony dynamics caused by the evolution of spatio-temporal heterogeneities in the system. Quenching effect I appears at the early stages of the colony growth irrespective of its type and, the higher the c_{MC}, the greater the dynamic viscosity of the medium and the larger the quenching effect I. The latter is also associated with the gradual cell proliferation inhibition as c_{MC} increases. It should be noted that the presence of MC could also affect cell–cell interactions by diminishing

the free space for the allocation of moving cells in the colony, an effect that would contribute to decreasing F and would also cooperate with quenching effect II in the noise term.

Quenching effect II appears once enlarged cells are formed at the colony border region. These cells tend to form groups that behave like slow-moving obstacles that become rate-determining of regular cell migration velocity. Regular cells follow long biased trajectories to reach the colony front, overtaking colony sites occupied by enlarged cells. It should be noted that the relative contribution of random and ballistic cell displacement characteristics to the cell motility mechanism remains almost the same either in the plain or the gel medium (Fig. 14). Histograms of directionality angles of cells at the colony border (Fig. 16) show that cell velocity in the direction of the colony front displacement decreases with time. This outstanding effect is consistent with the transition from the standard KPZ model in the plain medium to the QKPZ model in the gel medium.

In conclusion, new data provided by this work, within certain variable ranges, show links between continuous KPZ models interpreting the dynamic behavior of 2D Vero cell colony interfaces and cell-based Potts models used to deal with complex cell colony dynamics.

5 Conclusions

- The influence of spatio-temporal cell and colony morphology changes on quasi-linear and quasi-circular 2D Vero cell colony spreading dynamics in plain and MC-containing culture media (sols and gel) is described.
- For plain and MC-containing sol media, the spreading kinetics of quasi-circular colonies, with a small number of cells, fulfils a first-order rate equation in terms of either N or $<R>$, with average kinetic constants $<k_N>$ and $<k_R>$, respectively. At short t, the colony spreading is largely governed by cell mitosis, irrespective of c_{MC}. As c_{MC} increases, cell mitosis is gradually inhibited. At long times and in the gel medium, cell enlargement at the colony border mainly determines the colony front propagation rate and first-order kinetics, in terms of $<R>$, is observed.
- As the colony population increases, a constant $<v_F>$ front propagation regime is attained. Driving forces result from cell displacements, cell size increase, cell duplications and, probably to a lesser extent, from cell migration from inner 3D clusters to outer 2D domains.
- In the gel medium, the driving forces are mainly counterbalanced by two quenching effects (I and II), their relative contribution depending on N, c_{MC} and t. Quenching effect I is mainly caused by the medium structure coupled to mitosis inhibition and it manifests at all t.
- Quenching effect II appears at longer t when slow-moving, enlarged cells behave like obstacles, either like a quasi-compact (type II colony) or discontinuous (type III colony) barrier at the colony border region. Quenching effect II becomes of importance for type II and III colonies growing in the gel medium.
- Local cell size distribution and cell motility data are qualitatively consistent with some predictions of the extended cellular Potts models, particularly when considering mechanical cues for cell motility, cell density morphology-dependent distributions and effects of cell–cell adhesion.
- Cell motility characteristics change when going from plain to gel media. For the plain medium, the dynamics of the colony front roughness is characterized by a set of roughness

exponents compatible with the prediction of the standard KPZ model, whereas for the gel medium a QKPZ model is approached. The transition from the KPZ to the QKPZ 2D roughness dynamic regime can be related to the noise term mainly generated by quenching effect II. These effects are mainly manifested in the cell motility characteristics that change when going from plain to gel culture media.

Finally, results presented in this paper, obtained from colonies with different N, ages, initial geometries and growing in plain and MC-containing media, are qualitatively consistent with predictions of cellular Potts models and appear to be useful for describing processes at the cellular scale that explain the overall 2D front dynamics of large colonies, tackled by dynamic scaling analysis. Reported data complement previous results and encourage the search for correlations between global and microscopic approaches for further understanding of the behavior of complex systems.

Acknowledgments This work was supported by the Consejo Nacional de Investigaciones Cientficas y Técnicas of Argentina (PIP 2231 and PIP 0602) and the Comisión de Investigaciones Científicas (CIC), Pcia. Bs. As. We acknowledge Silvia Coronato for technical assistance.

References

1. Eming, S.A., Martin, P., Tomic-Canic, M.: Wound repair and regeneration: mechanisms, signaling, and translation. Sci Transl Med **6**, 265sr6 (2014)
2. Levental, K.R., Yu, H., Kass, L., Lakins, J.N., Egeblad, M., Erler, J.T., Fong, S.F.T., Csiszar, K., Giaccia, A., Weninger, W., Yamauchi, M., Gasser, D.L., Weaver, V.M.: Matrix crosslinking forces. Tumor progression by enhancing integrin signaling. Cell **139**, 891–906 (2009)
3. Barabasi, A.L., Stanley, H.E.: Fractal Concepts in Surface Growth. Cambridge University Press, Cambridge (1993)
4. Brú, A., Pastor, J.M., Fernud, I., Brú, I., Melle, S., Berenguer, C.: Super-rough dynamics on tumor growth. Phys Rev Lett **81**, 4008–4011 (1998)
5. Brú, A., Albertos, S., Subiza, J.L., García-Asenjo, J.L., Brú, I.: The universal dynamics of tumor growth. Biophys J **85**, 2948–2961 (2003)
6. Block, M., Schöll, E., Drasdo, D.: Classifying the expansion kinetics and critical surface dynamics of growing cell populations. Phys Rev Lett **99**, 248101 (2007)
7. Huergo, M.A.C., Pasquale, M.A., Bolzán, A.E., Arvia, A.J., González, P.H.: Morphology and dynamic scaling analysis of cell colonies with linear growth fronts. Phys Rev E **82**, 031903 (2010)
8. Huergo, M.A.C., Pasquale, M.A., Bolzán, A.E., González, P.H., Arvia, A.J.: Morphology and dynamic and morphology characteristics of cell colonies with radially spreading growth fronts. Phys Rev E **84**, 021917 (2011)
9. Huergo, M.A.C., Pasquale, M.A., Bolzán, A.E., González, P.H., Arvia, A.J.: Growth dynamics of cancer cell colonies and their comparison with noncancerous cells. Phys Rev E **85**, 011918 (2012)
10. Moglia, B., Guisoni, N., Albano, E.V.: Interfacial properties in a discrete model for tumor growth. Phys Rev E **87**, 032713 (2013)
11. Galeano, J., Buceta, J., Juarez, K., Pumariño, B., de la Torre, J., Iriondo, J.M.: Dynamical scaling analysis of plant callus growth. Europhys Lett **63**, 83–89 (2003)
12. Bonachela, J.A., Nadell, C.D., Xavier, J.B., Levin, S.A.: Universality in bacterial colonies. J Stat Phys **144**, 303–315 (2011)
13. Meakin, P.: Fractals, Scaling and Growth Far from Equilibrium. Cambridge University Press, Cambridge (1998)
14. Ahlers, M., Müller, W., Reichert, A., Ringsdorf, H., Venzmer, J.: Specific interactions of proteins with functional lipid monolayers—ways of simulating biomembrane processes. Angew Chem Int Ed Engl **29**, 1269–1285 (1990)

15. Takeuchi, K.A.: Experimental approaches to universal out-of-equilibrium scaling laws: turbulent liquid crystal and other developments. J Stat Mech (2014). doi:10.1088/1742-5468/2014/01/P01006
16. Huergo, M.A.C., Muzzio, N.E., Pasquale, M.A., González, P.H., Bolzán, A.E., Arvia, A.J.: Dynamic scaling analysis of two-dimensional cell colony fronts in a gel medium: a biological system approaching a quenched Kardar–Parisi–Zhang universality. Phys Rev E **90**, 022706 (2014)
17. Muzzio, N.E., Pasquale, M.A., González, P.H., Arvia, A.J.: Influence of individual cell motility on the 2D front roughness dynamics of tumour cell colonies. J Biol Phys **40**, 285–308 (2014)
18. Dan, D., Mueller, C., Chen, K., Glazier, J.A.: Solving the advection-diffusion equations in biological contexts using the cellular Potts model. Phys Rev E **72**, 041909 (2005)
19. Glazier, J.A., Graner, F.: Simulation of the differential adhesion driven rearrangement of biological cells. Phys Rev E **47**, 2128–2154 (1993)
20. Lushnikov, P.M., Chen, N., Alber, M.: Macroscopic dynamics of biological cells interacting via chemotaxis and direct contact. Phys Rev E **78**, 061904 (2008)
21. Turner, S., Sherrat, J.A., Painter, K.J., Saville, N.J.: From a discrete to a continuous model of biological cell movement. Phys Rev E **69**, 021910 (2004)
22. Cickovski, T., Huang, C., Chaturvedi, R., Glimm, T., Hentschel, H.G.E., Alber, M., Glazier, J.A., Newman, S.A., Izaguirre, J.A.: A framework for three-dimensional simulation of morphogenesis. ACM Trans Comput Biol Bioinform **2**, 273–288 (2005)
23. Chen, N., Glazier, J., Izaguirre, J., Alber, M.S.: A parallel implementation of the cellular Potts model for simulation of cell-based morphogenesis. Comput Phys Commun **176**, 670–681 (2007)
24. Thalhauser, C.J., Lowengrub, J.S., Stupack, D., Komarova, N.L.: Selection in spatial stochastic models of cancer: migration as a key modulator of fitness. Biol Direct **5**, 21 (2010). doi:10.1186/1745-6150-5-21
25. Wong, S.Y., Chiam, K.-H., Lim, C.T., Matsudaira, P.: Computational model of cell positioning: directed and collective migration in the intestinal crypt epithelium. J R Soc Interface **7**, S351–S363 (2010)
26. Izaguirre, J.A., Chaturvedi, R., Huang, C., Cickovski, T., Coffland, J., Thomas, G., Forgacs, G., Alber, M., Hentschel, G., Newman, S., Glazier, J.: CompuCell, a multi-model framework for simulation of morphogenesis. Bioinformatics **20**, 1129–1137 (2004)
27. Scianna, M., Preziosi, L., Wolf, K.: A cellular Potts model simulating cell migration on and in matrix environments. Math Biosci Eng **10**, 235–261 (2013)
28. Li, J.F., Lowengrub, J.: The effects of cell compressibility, motility and contact inhibition on the growth of tumor cell clusters using the cellular Potts model. J Theor Biol **343**, 79–91 (2014)
29. Lauffenburger, D.A., Horwitz, A.F.: Cell migration: a physically integrated molecular process. Cell **84**, 359–369 (1996)
30. Czirók, A., Varga, K., Méhes, E., Szabó, A.: Collective cell streams in epithelial monolayers depend on cell adhesion. New J Phys **15**, 075006 (2013)
31. Palieri, B., Bresler, Y., Wirtz, D., Grant, M.: Multiple scale model for cell migration in monolayers: elastic mismatch between cells enhances motility. Sci Rep **5**, 11745 (2015)
32. Lee, M.-H., Wu, P.-H., Staunton, J.R., Ros, R., Longmore, G.D., Wirtz, D.: Mismatch in mechanical and adhesive properties induces pulsating cancer cell migration in epithelial monolayer. Biophys J **102**, 2731–2741 (2012)
33. Treloar, K.K., Simpson, M.J., Haridas, P., Manton, K.J., Leavesley, D., Elwain, D.L.S.M., Baker, R.E.: Multiple types of data are required to identify the mechanisms influencing the spatial expansion of melanoma cell colonies. BMC Syst Biol **7**, 137 (2013)
34. Risser, R., Pollack, R.: A nonselective analysis of SV40 transformation of mouse 3T3 cells. Virology **59**, 477–489 (1974)
35. Ito, T., Ishikawa, Y., Okano, S., Hattori, T., Fujii, R., Shinozawa, T., Shibuya, A.: Cloning of human neuroblastoma cells in methylcellulose culture. Cancer Res **47**, 4146–4149 (1987)
36. Kobayashi, K., Huang, C.-I.: Thermoreversible gelation of aqueous methylcellulose solutions. Macromolecules **32**, 7070–7077 (1999)
37. Diambra, L., Cintra, L.C., Chen, Q., Schubert, D., Costa, L.D.F.: Cell adhesion protein decreases cell motion: statistical characterization of locomotion activity. Phys A **365**, 481–490 (2006)
38. Li, L., Wang, B.H., Wang, S., Moalim-Nour, L., Mohib, K., Lohnes, D., Wang, L.: Individual cell movement, asymmetric colony expansion, rho-associated kinase, and E-cadherin impact the clonogenicity of human embryonic stem cells. Biophys J **98**, 2442–2451 (2010)
39. Petitjean, L., Reffay, M., Grasland-Mongrain, E., Poujade, M., Ladoux, B., Buguin, A., Silberzan, P.: Velocity fields in a collectively migrating epithelium. Biophys J **88**, 1790–1800 (2010)
40. Thielicke, W., Stamhuis, E.: Towards user-friendly, affordable and accurate digital particle image velocimetry in MATLAB. J Open Res Software **2**, e30 (2014)

41. Radszuweit, M., Block, M., Hengstler, J.G., Schöll, E., Drasdo, D.: Comparing the growth kinetics of cell populations in two and three dimensions. Phys Rev E **79**, 051907 (2009)
42. Puliafito, A., Hufnagel, L., Neveu, P., Streichan, S., Sigal, A., Fygenson, D.K., Shraiman, B.I.: Collective and single cell behaviour in epithelial contact inhibition. Proc Natl Acad Sci U S A **109**, 739–744 (2012)
43. Friedl, P., Glimour, D.: Collective cell migration in morphogenesis, regeneration and cancer. Nat Rev **10**, 445–457 (2009)
44. Haque, A., Morris, E.R.: Xanthan-like "weak gel" rheology from dispersions of ispaghula seed husk. Carbohydr Polym **22**, 223–232 (1993)
45. Sarkar, N.: Kinetics of thermal gelation of methylcellulose and hydroxy-propyl-methylcellulose in aqueous solutions. Carbohydr Polym **26**, 195–203 (1995)
46. Li, L., Thangamathesvaran, P.M., Yue, C.Y., Tam, K.C., Hu, X., Lam, Y.C.: Gel network structure of methylcellulose in water. Langmuir **17**, 8062–8068 (2001)
47. Szabó, A., Unnep, R., Méhes, E., Twal, W.O., Argraves, W.S., Cao, Y., Czirók, A.: Collective cell motion in endothelial monolayers. Phys Biol **7**, 046007 (2010)
48. Medzon, E.L., Merchant, D.J.: Interaction of the LM cell surface with methylcellulose and vaccinia virus. Mode of action and implications for large scale vaccine production. In Vitro **7**, 46–58 (1971)
49. Kardar, M., Parisi, G., Zhang, Y.-C.: Dynamic scaling of growing interfaces. Phys Rev Lett **56**, 889–892 (1986)
50. Parisi, G.: On surface growth in random media. Europhys Lett **17**, 673–678 (1992)
51. Sneppen, K.: Self-organized pinning and interface growth in a random medium. Phys Rev Lett **69**, 3539–3542 (1992)